Simulation of stimulated Raman adiabatic passage from the 1*S* to the 2*S* states of the hydrogen and antihydrogen atoms

AbdAlGhaffar K. Amer,[1,*] A. Capra,[2] T. Friesen,[3] M. C. Fujiwara,[2] T. Momose,[2,4] C. So,[2,3] and F. Robicheaux[1,†]

[1]*Department of Physics and Astronomy, Purdue University, West Lafayette, Indiana 47906, USA*

[2]*TRIUMF, 4004 Wesbrook Mall, Vancouver, British Columbia, Canada V6T 2A3*

[3]*Department of Physics and Astronomy, University of Calgary, Calgary, Alberta, Canada T2N 1N4*

[4]*Department of Chemistry, University of British Columbia, Vancouver, British Columbia, Canada V6T 1Z1*

(Received 11 March 2025; accepted 16 September 2025; published 10 October 2025)

Achieving a high population of antihydrogen and hydrogen atoms in the 2*S* level is essential for spectroscopy measurements testing similarities between matter and antimatter. We propose and examine the efficiency of applying the STIRAP (stimulated Raman adiabatic passage) process in achieving high population transfer from the 1*S* to the 2*S* levels. We utilized a circularly polarized Lyman alpha (Ly-α) pulse to couple the 1*S* state to the 2*P* state and a microwave pulse to couple the 2*P* state and the 2*S* state. We calculate the efficiency of the STIRAP process for transferring the population between the stretched states ($1S_d, 2S_d$) as a function of experimental parameters such as Rabi frequencies and pulse durations. We find that a Ly-α pulse with an energy of a few nanojoules could produce nearly perfect transfer at zero detunings for atoms on the laser beam axis. We extended the analysis to a thermal ensemble of atoms, where Doppler detuning affects the velocity distribution of the hydrogen atoms produced in the 2*S* level. We found that the width of such velocity distribution is controlled by the Rabi frequency. We show that the peak velocity of the hydrogen atoms in the 2*S* level after STIRAP can be controlled by the Ly-α pulse detuning. The efficiency of STIRAP in transferring population increases at low temperature ($T \sim 1$ mK). Finally, we show that a background magnetic field improves the transfer rates between the other trappable states ($1S_c, 2S_c$).

DOI: 10.1103/wx74-xg4j

I. INTRODUCTION

The 2*S* level of the hydrogen atom is a metastable state with a lifetime of 0.12 s, which is about eight orders of magnitude longer than the 2*P* state [1]. The 1*S*-2*S* transition is a good candidate for precision measurement experiments [2]. For instance, it is used in testing the CPT (charge conjugation, parity, and time reversal) symmetry of the standard model [3]. These tests are achieved by comparing the different fine and hyperfine splittings of the hydrogen and antihydrogen atoms [4–6]. Besides increasing the accuracy of the 1*S*-2*S* transition frequency, future experiments to evaluate the antihydrogen Rydberg constant as well as the antiproton radius require two independent transition frequency measurements. A good candidate for such measurements are transitions from the 2*S* level to higher levels of the antihydrogen atoms. These measurements would benefit from a large population of antihydrogen atoms in the 2*S* level. One of the aims of this work is to show that the stimulated Raman adiabatic passage (STIRAP) process could produce useful populations of atoms in the 2*S* level with lower pulse intensities and thus negligible ionization rates.

Typically, the 1*S*-2*S* transition of the hydrogen atom is achieved by using two counterpropagating photons of wavelength 243 nm each [1,7]. This approach removes the net first-order Doppler shift; thus it mostly eliminates the Doppler broadening effects and produces a narrow transition linewidth. Additionally, the hydrogen atoms do not experience recoil when absorbing the two counterpropagating photons. Therefore, this scheme is useful for spectroscopy measurements of the 1*S*-2*S* transition. However, when the aim is to produce a large population of hydrogen atoms in the 2*S* level, it can face some challenges. For instance, the 1*S*-2*S* transition is highly nonresonant in the first 243 nm photon of this scheme. Thus the transition requires high laser intensities and energies [1,5] reaching orders of magnitude 10^7 W m^{-2} and 10^{-3} J, respectively, for meaningful transition probabilities. At such high intensities, the rate of photoionization from the 2*S* state becomes high [8], thus reducing the efficiency of the 1*S*-2*S* transfer process. The current efficiency of such a scheme in the literature is about 0.1% [8]. However, as far as we know, that technique has not been optimized to produce maximum population transfer. Other studies have investigated population transfer through the continuum [9–11]. However, in [11] it was shown that when such technique is applied to hydrogen, the ionization rates are comparable to those seen in the 243 nm photons scheme.

In this work, we simulate the implementation of a STIRAP process to transfer hydrogen or antihydrogen atoms from the 1*S* to the 2*S* level. We use the 2*P* level as the intermediate state, relying on the resonant dipole transitions between the 2*P* levels and both the initial 1*S* and the target 2*S* levels. Two radiation pulses are utilized; the probe (P) pulse, which is a Lyman alpha pulse (Ly-α), that couples the 1*S* and the 2*P* levels and a

*Contact author: amer1@purdue.edu

†Contact author: robichf@purdue.edu

Stokes (S) pulse which is a microwave pulse that couples the $2P$ and the $2S$ levels. The required Ly-α pulse has intensities of $\sim 10^4\,\mathrm{W\,m^{-2}}$ and energies of $\sim 10^{-9}\,\mathrm{J}$, several orders of magnitude less than those used in the 243 nm two-photon excitation. Consequently, the ionization probability becomes negligible (of order 10^{-8} of the excited atoms). A possible limitation to applying STIRAP to this system is the high decay rate from the intermediate $2P$ level to the ground state compared to the almost negligible decay rate into the $2S$ level. This high decay rate, as well as the disparity in the branching ratios, is known to reduce the efficiency of the STIRAP process [12]. Another possible limitation of applying this approach is that the Doppler shift experienced by the Ly-α pulse is five orders of magnitude higher than that experienced by the microwave pulse connecting the $2S$ and the $2P$ levels [13]. For thermal ensembles of hydrogen atoms at millikelvin temperatures, this shift results in single- and two-photon detunings comparable to transition widths of interest. This affects the efficiency of the STIRAP process in transferring populations into the $2S$ level for higher-temperature experiments. On the plus side, the Doppler effect can also be used to generate a population of atoms in the $2S$ level with a specific range of velocities, Sec. III B 1. Previous studies have been conducted on the velocity distribution of atomic systems after STIRAP for cooling purposes [14–16].

In this paper, we show the feasibility of using STIRAP to transfer population to the $2S$ hydrogen atom level. In the Methods section, Sec. II, we introduce the setup of the STIRAP process for a single hydrogen atom. We start with presenting the Lindbladian for the STIRAP process between the stretched states $(1S_d, 2S_d)$ in Sec. II A. Then, in Sec. II B, we discuss the approximate method we implement to obtain the velocity distribution of the atoms after the STIRAP process, including the recoil effects from absorbing the Ly-α photon as well as the decay from the intermediate state. Later, in Sec. II C, we discuss how the presence of a magnetic field affects the STIRAP Hamiltonian. Section III is the Results section where we discuss the efficiency of applying the STIRAP approach in producing an appreciable transfer of population from the $1S$ level to the $2S$ level given the properties of the atom cloud and the geometric shape of the STIRAP beams. We divide it into three parts. We start in Sec. III A by analyzing the features of the single-atomic system with emphasis on the ones relevant to understanding the bulk of atoms behavior. Section III B discusses the velocity distribution of the hydrogen atoms in both the $1S$ and the $2S$ levels after the STIRAP process. In Sec. III C we show that the presence of a magnetic field can improve the STIRAP process between the non-stretched states $(1S_c, 2S_c)$ with relatively little loss in the hydrogen atoms. We will use "hydrogen" atom in all that follows to refer to both hydrogen and antihydrogen with the understanding that for antihydrogen, the spins are flipped to obtain the states with the appropriate properties in a magnetic field.

II. METHODS

A. Treatment of STIRAP between the 1S and 2S states of hydrogen

To transfer population from the $1S$ to the $2S$ level using STIRAP, we couple these levels through the intermediate $2P$ states using two pulses; a probe pulse and a Stokes pulse [17]. A Λ linkage is constructed using the $2P$ states with a fine structure total angular momentum ($J = 3/2$). The $2P$ states with fine structure total angular momentum ($J = 1/2$) are detuned enough that the coupling to them is negligible; we tested this by numerical calculations in addition to simple estimates from Rabi frequencies and detunings. The probe (P) pulse is the Lyman alpha pulse (Ly-α), that couples the $1S$ triplet ($F = 1$) and the $2P$ fine structure state with the electron total angular momentum ($J = 3/2$) as illustrated in Fig. 1. In our simulations, we take the P pulse to be circularly polarized with a Gaussian profile in time, such that

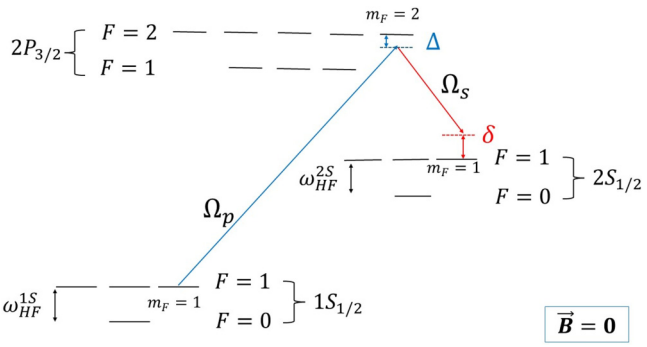

FIG. 1. An illustration of the transitions of interest with the $1S$ and $2S$ hyperfine splitting; $\omega_{\mathrm{HF}}^{1S} = 2\pi\times 1.42\times 10^9$ rad/s, $\omega_{\mathrm{HF}}^{2S} = 2\pi\times 0.177\times 10^9$ rad/s [13,18] not drawn to scale. The $2P$ hyperfine splitting is much smaller (23 MHz) and also not drawn to scale. The pump pulse is the Ly-α pulse with frequency $\omega_\alpha = 2\pi\times 2.466\times 10^{15}$ rad/s, and the Stokes pulse is a microwave pulse with frequency $\omega_s = 0.978\times 2\pi\times 10^{10}$ rad/s. In the Λ scheme $\Delta = \delta_p$ and $\delta = \delta_p - \delta_s$, where δ_p and δ_s are the P pulse and the S pulse detunings, respectively, with δ_p as defined in Eq. (1). The $2P$ states with electron angular momentum $J = \frac{1}{2}$ are detuned by about 11 GHz so their contributions are negligible.

$$\vec{E}_p(t) = -\mathfrak{Re}\big(E_p^0 e^{-i(\omega_\alpha+\delta_p)t} e^{-(2\ln 2)(t-t_0^p)^2/\tau^2}\hat{\epsilon}_+\big), \qquad (1)$$

with the unit vector $\hat{\epsilon}_+ = \frac{-1}{\sqrt{2}}(\hat{x} + i\hat{y})$; E_p^0 is the amplitude of the electric field; the Ly-α transition angular frequency $\omega_\alpha = 2\pi\times 2.466\times 10^{15}$ rad/s [13]; δ_p is the detuning in the angular frequency; the FWHM of the intensity duration, τ, was taken to be 20 ns in all our simulations to be similar to the expected timescale in the proposed HAICU experiments. The pulse also has a Gaussian radial profile with the maximum amplitude of the electric field E_p^0 given by

$$E_p^0 = \sqrt{\frac{\mathcal{E}}{w_0^2\tau}}\sqrt{\frac{4(2\sqrt{\ln 2})}{\epsilon_0 c\pi^{3/2}}}, \qquad (2)$$

where w_0 is the waist of the Gaussian pulse, $\mathcal{E}$ is the energy in the pulse, c is the speed of light, and ϵ_0 is the permittivity of free space. In many simulations, we used a pulse waist $w_0 = 2\,\mathrm{mm}$ and a total energy of 3 nJ. We made such choices for the pulse parameters to match those proposed in experiments on trapped hydrogen and antihydrogen atoms for the HAICU project [19,20] at TRIUMF (Vancouver, Canada). This pulse produces a Hamiltonian matrix element, as shown

in Appendix A 1, of the form

$$H_{12}(t) = -\hbar\Omega_p(t)/2 = \langle\psi_{100}|e\vec{E}_p(t)\cdot\vec{r}|\psi_{211}\rangle$$
$$= -\frac{eE_p^0}{\sqrt{3}}\langle R_{10}(r)|r|R_{21}(r)\rangle e^{-(2\ln 2)(t-t_0^p)^2/\tau^2}$$
$$= -\frac{\hbar\Omega_p^0}{2}e^{-(2\ln 2)(t-t_0^p)^2/\tau^2}, \quad (3)$$

where t_0^p is the time at which the Gaussian pulse reaches its peak and R_{nl} is the radial part of the hydrogen eigenstates ψ_{nlm}. This gives a peak Rabi frequency of the P pulse $\Omega_p^0 = 4.915\times10^8$ rad/s. When discussing ensembles of trapped atoms in Sec. III B 1 we will average over the atom's position within the radial profile of the pulse.

The Stokes (S) pulse is a microwave pulse that couples the $2P$ states ($J = 3/2$) with the $2S$ hyperfine states and has an angular frequency $\omega_s = 0.978\times2\pi\times10^{10}$ rad/s and a detuning δ_s. We used the same electric-field polarization for the S pulse as that for the P pulse, Eq. (1), but with a different amplitude E_s^0 instead of the amplitude of the P pulse, E_p^0. We also use a Gaussian time dependence for the S pulse which gives a Hamiltonian matrix element of the form

$$H_{23}(t) = -\hbar\Omega_s(t)/2$$
$$= -\frac{\hbar\Omega_s^0}{2}e^{-(2\ln 2)t^2/\sigma^2}, \quad (4)$$

where Ω_s^0 and σ are the parameters controlling the strength and the duration of the S pulse, respectively. In most of the simulations presented in this paper Ω_s^0 is of the same order of magnitude as Ω_p^0. As typically known for efficient STIRAP [17,21] the parameters σ and t_0^p need to be tuned such that the pump-Stokes offset [21] creates a "counterintuitive" ordering of the pulses with the S pulse preceding the P pulse and a sufficient overlap between them. As the parameters deviate from such optimum configuration, the efficiency of the STIRAP process in transferring population decreases, and more population moves into the radiative intermediate state. An example of the time dependence of the two pulses is shown in Fig. 2. These pulses are more closely spaced in time than is typical for STIRAP, as will be discussed in Sec. III A. Unlike the P pulse, the microwave S pulse is not a Gaussian pulse in the radial direction; rather, we assume that its amplitude is approximately unchanged over the sample size of the hydrogen atoms.

In the complete treatment of the STIRAP process, there are 16 possible states in the system, namely, four hyperfine states for the $1S$ level, 4×2 states for the $2P$ ($J = 3/2$) level, and four hyperfine states for the $2S$ level as illustrated in Fig. 1. However, the circularly polarized pulses, Eq. (1), impose well-known selection rules for a rank 1 tensor operator [22]. Due to these selection rules, only five of the $2P$ level states (F, m_F) couple to the S level states, namely, the $2P$ states, $\{(2,2),(2,1),(2,0),(1,1),(1,0)\}$, thus resulting in only 13 of the 16 possible states being accessible through the circularly polarized pulses. Thus the STIRAP Hamiltonian will be a matrix of dimensions 13×13.

In order to include the decay from the $2P$ states to the $1S$ states we use the Lindblad master equation for the density matrix of the system ρ:

$$\dot{\rho} = \frac{-i}{\hbar}[H,\rho] - \sum_n \Gamma_n((L_n^\dagger L_n\rho + \rho L_n^\dagger L_n)/2 - L_n\rho L_n^\dagger), \quad (5)$$

with H being the hermitian STIRAP Hamiltonian and Γ_n are the decay rates from the $2P$ to the $1S$ states for each decay channel. They are proportional to the square of the expectation value of the dipole matrix element connecting the initial and final states [23]. The L_n matrices are 13×13 dimensional jump operators. They transfer population from the $2P$ states to the relevant $1S$ states with the decay rate Γ_n as defined in Appendix B.

Generally, the STIRAP Hamiltonian couples each $1S$ hyperfine eigenstate to multiple $2P$ hyperfine eigenstates. By explicit evaluation of the Hamiltonian, one observes that the stretched state $1S_d$ ($F = 1$, $m_F = 1$) only couples to the $2P_a^\uparrow$ ($F = 2$, $m_F = 2$) which only couples through the S pulse to the states $2S_d$ ($F = 1$, $m_F = 1$). Thus those three states form a closed system under the Hamiltonian part of the time

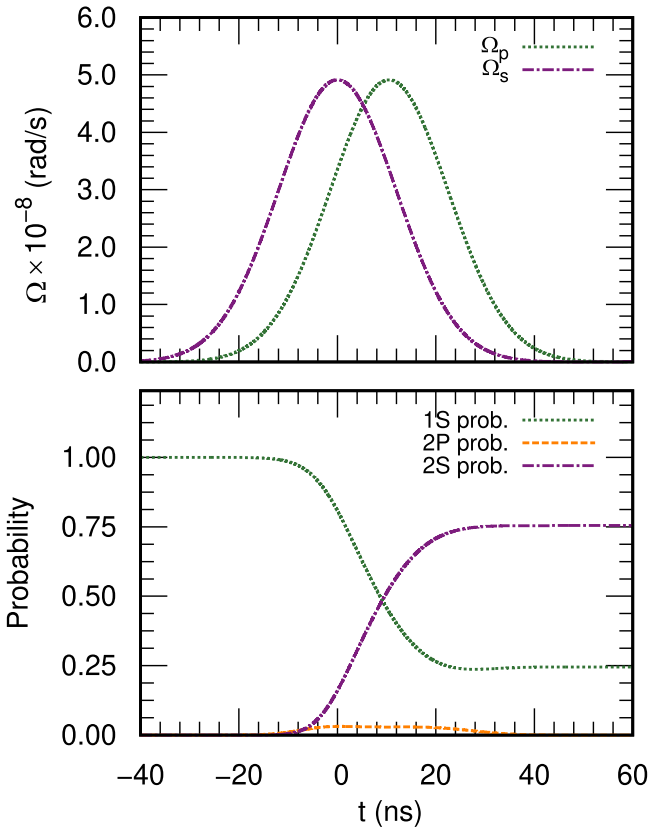

FIG. 2. The S and P pulses as well as the state $\{1S_d, 2P_a^\uparrow, 2S_d\}$ probabilities as a function of time for typical experimental parameters and zero pulses detunings. The P pulse is the Gaussian in Eq. (3) with $t_0^p = 10.5$ ns. The S pulse follows Eq. (4) with $\sigma = \tau = 20$ ns and $\Omega_s^0 = \Omega_p^0 = 4.915\times10^8$ rad/s. The maximum population in the $2P$ state is about 3% which shows that the system is close to adiabatic.

evolution with the effective 3×3 STIRAP Hamiltonian:

$$\mathcal{H}(t) = -\hbar \begin{pmatrix} 0 & \frac{\Omega_p}{2} & 0 \\ \frac{\Omega_p}{2} & \Delta & \frac{\Omega_s}{2} \\ 0 & \frac{\Omega_s}{2} & \delta \end{pmatrix}(t), \tag{6}$$

where $\{\Delta, \delta\}$ are the single-photon and the two-photon detuning, respectively; see the caption of Fig. 1. Similarly, the $2P_a^{\uparrow}$ state can only decay to the $1S_d$, contrary to the other $2P$ states that could decay to multiple states of the $1S$ level. Consequently if the hydrogen atoms are initialized in the $1S_d$ state, then the time evolution of the density matrix under the full master equation does not move population outside the three states: $1S_d$, $2P_a^{\uparrow}$, and $2S_d$. Consequently, we can reduce the treatment of the problem to a three-state subsystem constructed from these states.

We work in this 3×3 subspace as we examine the efficiency of the STIRAP process and its dependence on the different experimental parameters. In Sec. III C we show that a magnetic field can help selectively transfer population between the other trappable nonstretched states, $1S_c$ and $2S_c$. That is achieved by making the subspace of interest approximately closed. Finally, we note that, in the absence of a magnetic field, the usage of laser pulses with the opposite circular polarization would only flip the total angular momentum F of the states involved in the STIRAP process.

B. Thermal distribution and recoil effects

In the previous section, the discussion did not include the center of mass motion of the hydrogen atom. In Appendix A 2 we show the change in the STIRAP Hamiltonian when we work with a tensor product of the internal states and the center of mass momentum state in the direction of the incident Ly-α photon $|k\rangle$. In the literature, there has been work on the use of STIRAP processes in atomic systems for cooling [14–16]. Here, we present the numerical technique we used to study the velocity distributions of the atoms after the STIRAP process in both the initial and the target states. This atomic system gains an effective momentum kick from the STIRAP process as well as from the decay of the intermediate state, which are both accounted for as follows.

We restrict the analysis to the states $\{1S_d \otimes |k\rangle, 2P_a^{\uparrow} \otimes |k + k_\alpha\rangle, 2S_d \otimes |k + k_\alpha\rangle\}$, where the first part is the internal state of the hydrogen atom and the second part is the center of mass momentum state in the direction of the incident photon. The states with the principle quantum number $n = 2$ have gained a momentum kick $\hbar k_\alpha = 2\pi\hbar/(121.6\times10^{-9}\,\mathrm{m})$ from absorbing the Ly-α photon.

In Appendix A 2, we derive the Hamiltonian for a hydrogen atom with an arbitrary initial momentum $\hbar k$. The full density matrix of an atom in the thermal distribution would have different initial momenta for the $1S$ state, sampled from a Maxwell-Boltzmann distribution. In order for the density matrix to describe the entire system, we expand it to become $3M\times3M$, where M is the number of the different allowed initial momenta $\hbar k$. We only keep track of the component of the momentum that is parallel to the incident P pulse. The momentum states have a grid spacing $\hbar\delta k$ in the interval $k \in [-k_{\max} : k_{\max}]$.

In the simulation $k_{\max}$ is chosen based on the temperature of the initial hydrogen atoms such that all accessible momentum states are included. The momentum grid spacing $\hbar\delta k$ is chosen to be sufficiently smaller than the recoil momentum $\hbar k_\alpha$ as discussed in Sec. III B.

The decay transfers population from the state $2P_a^{\uparrow} \otimes |k + k_\alpha\rangle$ to the state $1S_d \otimes |k'\rangle$, where k' could take values in the range $[k : k + 2k_\alpha]$. The exact value of momentum of the hydrogen atom after emitting a photon depends on the direction of the emitted photon compared to the atom momentum. A crude approximation would be to use the average outcome of multiple decay channels. Since hydrogen atoms are equally likely to emit a photon in the forward and the backward directions, the average effect would be no change in the momentum of hydrogen atoms after decaying to the $1S$ state, i.e., $k' = k + k_\alpha$. We term this the "averaged approach."

An improvement to this approximation is to allow the photon to be emitted in all directions, following the known angular distribution of dipole radiation $1 + \cos(\theta)^2$ [24], with $\cos(\theta) = -(k' - k - k_\alpha)/k_\alpha$. Thus the probability of the hydrogen atom $2P$ state to decay with momentum $\hbar(k + k_\alpha)$ into a $1S$ state with momentum $\hbar k'$ would be

$$\xi(k') = \frac{3}{8k_\alpha}\int_{k'-\delta k/2}^{k'+\delta k/2}(1 + f(\bar{k})^2)d\bar{k}, \tag{7}$$

where $f(\bar{k}) = (\bar{k} - k - k_\alpha)/k_\alpha$ and δk is the momentum spacing of the density matrix in the simulation and $\bar{k} \in [k : k + 2k_\alpha]$. The simulations converged for $\delta k \simeq k_\alpha/20$. For later discussions, we term this approach with a quantized momentum grid the "quantized approach". In Sec. III B we compare the resulting thermal distributions from the crude "averaged approach" and the quantized approach.

C. Adding magnetic field effects

The feasibility of using magnetic fields to selectively control the transfer between magnetic sublevels has been explored earlier [25–27]. For a hydrogen atom in the presence of a background magnetic field, the Hamiltonian of the system changes to

$$\hat{H} = \hat{H}_0 + \frac{g_e e}{2m_e}\vec{B}\cdot\hat{\vec{S}}_e - \frac{g_p e}{2m_p}\vec{B}\cdot\hat{\vec{S}}_p, \tag{8}$$

where $\hat{H}_0$ is the hydrogen atom Hamiltonian without the magnetic field; e is the elementary charge; m_e the electron mass; m_p the proton mass; $\{\hat{\vec{S}}_e, \hat{\vec{S}}_p\}$ are the spin operators for the electron and the proton, respectively; and $\{g_e, g_p\}$ are the g factor for the gyromagnetic ratios of the electron and the proton, respectively. Due to the coupling to the magnetic field, the hyperfine states of the $1S$ and the $2S$ states are mixed. The eigenstates and their eigenvalues as a function of the magnetic field are found analytically using the Breit-Rabi formula. The stretched states discussed in the previous sections, $1S_d$, $2P_a^{\uparrow}$, and $2S_d$, will remain a closed system with the magnetic field only introducing shifts in the transition frequencies. In this subsection we treat the evolution of the system starting from the trappable $1S_c$ state to the $2S_c$ state through the $2P_a^{\downarrow}$ state with $(-1/2)$ proton spin. The states are given in terms of a tensor product between the orbital state $|n, l, m\rangle$ and the z component's spin states of the electron and the proton $|s_z^e, s_z^p\rangle$

as follows:

$$
\begin{aligned}
1S_c &= |1,0,0\rangle \otimes (\beta_{1S}|1/2,-1/2\rangle + \alpha_{1S}|-1/2,1/2\rangle),\\
2P_a^{\downarrow} &= |2,1,1\rangle \otimes |1/2,-1/2\rangle,\\
2S_c &= |2,0,0\rangle \otimes (\beta_{2S}|1/2,-1/2\rangle + \alpha_{2S}|-1/2,1/2\rangle),
\end{aligned} \tag{9}
$$

with

$$
\begin{aligned}
\beta_n^2 &= \frac{1}{2} + \frac{B\mu_+}{\sqrt{4B^2\mu_+^2 + \hbar^2\omega_{\mathrm{HF}}^n}},\\
\alpha_n^2 &= \frac{1}{2} - \frac{B\mu_+}{\sqrt{4B^2\mu_+^2 + \hbar^2\omega_{\mathrm{HF}}^n}},
\end{aligned} \tag{10}
$$

where ω_{HF}^n are the hyperfine splittings in Fig. 1 with the index n going over the $1S$ and the $2S$ levels and

$$
\mu_+ = \frac{g_e e}{8m_e} + \frac{g_p e}{8m_p}. \tag{11}
$$

The values of the $\{\alpha_n^2, \beta_n^2\}$ give the probability that the electron has a spin-up or spin-down, respectively. Thus when evaluating the dipole matrix element in Eq. (3) for the STIRAP process, the matrix element coupling the $2P_a^{\downarrow}$ and the $1S_c$ states will have a factor of β_{1S} while that coupling the $2P_a^{\downarrow}$ and the $2S_c$ states will have a β_{2S} factor.

The STIRAP Hamiltonian terms are thus dependent on the magnetic field:

$$
H(t) = \hbar \begin{pmatrix} E^{1S}(B) & -\frac{\Omega_p}{2}\beta_{1S} & 0 \\ -\frac{\Omega_p}{2}\beta_{1S} & -\Delta + 2B\frac{g_e e}{\hbar m_e} & -\frac{\Omega_s}{2}\beta_{2S} \\ 0 & -\frac{\Omega_s}{2}\beta_{2S} & -\delta + E^{2S}(B) \end{pmatrix}(t), \tag{12}
$$

with

$$
E^n(B) = -\frac{\omega_{\mathrm{HF}}^n}{2} + \frac{\sqrt{4B^2\mu_+^2 + \hbar^2\left(\omega_{\mathrm{HF}}^n\right)^2}}{2\hbar}, \tag{13}
$$

where again the index n goes over the $1S$ and the $2S$ levels. The Hamiltonian could be put in a simpler form by subtracting $E^n(B)$ and redefining the detuning to become

$$
H(t) = -\hbar \begin{pmatrix} 0 & \frac{\Omega_p}{2}\beta_{1S} & 0 \\ \frac{\Omega_p}{2}\beta_{1S} & \bar{\Delta}(B) & \frac{\Omega_s}{2}\beta_{2S} \\ 0 & \frac{\Omega_s}{2}\beta_{2S} & \bar{\delta}(B) \end{pmatrix}(t), \tag{14}
$$

where now

$$
\begin{aligned}
\bar{\Delta}(B) &= \Delta - 2B\frac{g_e e}{\hbar m_e} + E^{1S}(B),\\
\bar{\delta}(B) &= \delta - E^{2S}(B) + E^{1S}(B).
\end{aligned} \tag{15}
$$

The other effect of the magnetic field is the change in the branching ratios of the $2P$ state when decaying into the $1S$ sublevels. Since the decay rate from $2P_a^{\downarrow}$ to $1S_c$ is proportional to the square of the dipole matrix element that connects them, the decay rate into the $1S_c$ state becomes $\Gamma_0 \times \beta_{1S}^2$ where Γ_0 is as defined in Appendix B. The decay into the $1S_a$ state has the branching ratio $(1-\beta_{1S}^2)$. However, the $1S_a$ to the $2P_a^{\downarrow}$ transition is far from resonance so the $1S_a$ behaves as a dark state with a negligible percentage of atoms getting back from it into the $\{1S_c, 2P_a^{\downarrow}, 2S_c\}$ subsystem.

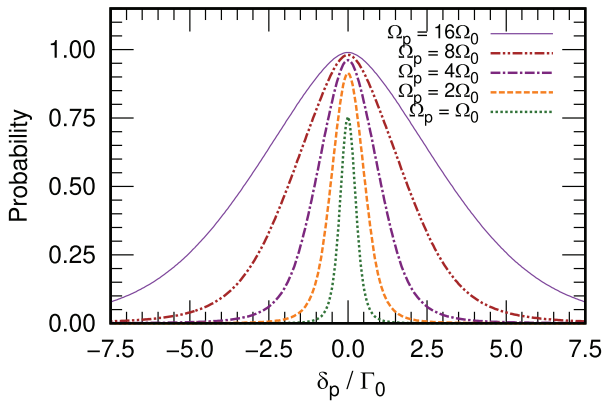

FIG. 3. The final probability to be in the $2S_d$ state as a function of the P pulse detuning δ_p for the Rabi frequencies of the S and P pulses $\Omega_p^0 = \Omega_s^0 = \{1,2,4,8,16\}\times\Omega_0$, with $\Omega_0 = 4.915\times10^8$ rad/s. The simulations were run while keeping the microwave pulse detuning δ_s as well as the pulses duration $\tau = \sigma = 20$ ns fixed, thus changing the Ly-α pulse energy. The transfer rate to the $2S$ level drops for δ_p outside the range $[-\Omega_p^0 : \Omega_p^0]$.

Finally we note that in this section effects like the difference between the g_e factor in the levels with the principle quantum numbers, $n=1$ and $n=2$, as well as the diamagnetic potential term from the magnetic field, were neglected, as both of them introduce energy changes of the order of a few kilohertz [8] which result in much less than a percent change in the final populations; see Fig. 3.

III. SIMULATION RESULTS

Here we discuss the simulation results as we progressively add effects to the STIRAP process. In Sec. III A, we study the efficiency of the STIRAP process in transferring the population between the stretched states $\{1S_d, 2S_d\}$, when the atoms are held in space and no recoil effects are included. These two restrictions lead to cases where ∼100% of the population can be transferred to the $2S$ state. We vary physical parameters such as the detuning of each pulse and the Rabi frequency. In most of the simulations the STIRAP efficiency is limited by the realistic energy achievable by a Ly-α pulse in a setup like HAICU. In Sec. III B we analyze the STIRAP process for thermal ensembles of hydrogen atoms; the resulting Doppler width for achievable temperatures can strongly reduce the fraction transferred into the $2S$ state. We also study how the change in the hydrogen atoms' temperatures affects the transfer rates of STIRAP as well as the velocity distribution of the resulting hydrogen atoms in the $2S$ level. In Sec. III B 2 we study the dependence of the number of atoms going through STIRAP from a spatially extended sample on the P pulse's waist and energy with the spatial Gaussian profile of the Ly-α beam taken into account. Allowing the atoms to not be at the center of the Ly-α beam further reduces the population transferred into the $2S$ state and necessitates the introduction of a parameter analogous to a cross section per laser shot. In Sec. III C we treat the STIRAP between the states $\{1S_c, 2S_c\}$ with a background magnetic field that changes the efficiency

of the transition due to the changing composition of the $1S_c$ state, Eq. (9).

A. Stationary single-atom $1S_d \rightarrow 2S_d$ STIRAP

Having made experimentally motivated choices for the parameters of the P pulse, Ω_p^0, τ, and the pulse waist w_0, there remain other experimental parameters that could be tuned to produce an efficient STIRAP process, namely, $\{\Omega_s^0, \sigma, t_0^p\}$. To understand the effects of these parameters, we investigate the ideal case in which the atoms are fixed in space at the center of the Ly-α beam. In order to know what values for these parameters would produce an effective STIRAP process, we initialized the hydrogen atom in the $1S_d$ state and swept the values of those parameters over the ranges $\Omega_s^0 \in (0:5]\Omega_p^0$, $\sigma \in (0:10]\tau$, and $t_0^p \in (0:2]\sigma$. The optimum values for these parameters were found to be $\Omega_s^0 = \Omega_p^0$, $\sigma = \tau$. The optimal pulse delay was found to be $t_0^p = 10.5$ ns $\sim 0.525\tau$, which is smaller than $\sim 0.85\tau$ which is typical in the literature [28]. This difference is attributed to the high decay rate of the $2P$ level, Appendix B, as well as the disparity in its branching ratios to the $1S$ states compared to the negligible decays into the $2S$ states. To test that, we ran separate simulations for smaller decay rates $\sim 0.01\Gamma_0$ and equal branching ratios, and both lead to more population transfer to the $2S$ level at larger pulse separations when keeping the other pulse parameters fixed. The case of equal branching ratios had better agreement with the $\sim 0.85\tau$ in the literature [17]. However, for the decay rates and the branching ratios of the $2P$ states of the hydrogen atom, Appendix B, a pulses separation of $t_0^p = 10.5$ ns $\sim 0.525\tau$ gave the best population transfer into the $2S$ level. We examined implementing microwave pulses proportional to e^{-t^4/σ^4} and obtained results similar to a Gaussian pulse. Unless otherwise indicated, we use the pulses parameters listed in this paragraph for the rest of the simulations in this work.

Since in our system $\Gamma_0 \gtrsim \Omega_0$, the analysis in [12] works well in characterizing the adiabaticity domain of the system, where the STIRAP efficiency improves exponentially in $(\Omega_p^0)^2 \times \tau/\Gamma_0$. In Fig. 2 we show the S and P pulses of the STIRAP process as well as the time evolution of the probability of being in each of the three states as a function of time at zero detunings for both pulses. For these Rabi frequencies, the system falls into the adiabaticity domain where $\Omega_p^0 \times \tau > 3\pi$ and $(\Omega_p^0)^2 \times \tau/\Gamma_0 = 7.69 > 1$ [12,17]. The STIRAP process transfer rate efficiency is about 75%. The efficiency falls short of a $\sim$90% transfer rate, because the intermediate state decays only into the initial state. This disparity in the intermediate state decay rates was shown to decrease the efficiency of the STIRAP process in [12]. However, this efficiency can be enhanced by increasing the pulse energy; see Figs. 3 and 5.

To better understand the linewidth of the produced $2S$ atoms of a thermal ensemble of hydrogen atoms, Sec. III B, we examine the efficiency of the STIRAP process as the pulses detuning is varied. Since the Doppler detuning $\Delta_D = \vec{v} \cdot \vec{k}$ of the Ly-α is five orders of magnitude higher than that of the microwave pulse, we only sweep the P pulse detuning while keeping the S pulse detuning fixed. We study the behavior of the system for $\Omega_s^0 = \Omega_p^0$ and both are equal to multiples of the Rabi frequency $\Omega_0 = 4.915 \times 10^8$ rad/s. In Fig. 3 we see

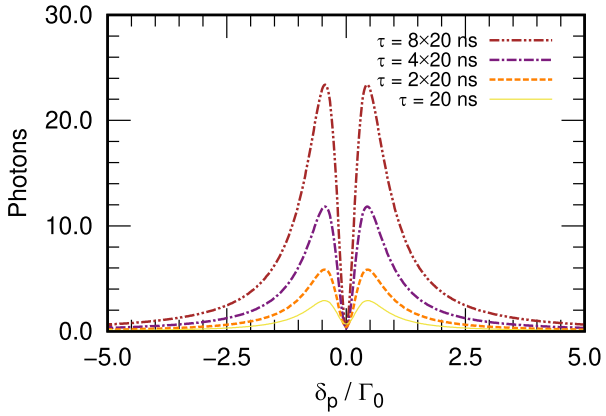

FIG. 4. The number of emitted photons as a function of the P pulse detuning δ_p while keeping the microwave pulse detuning δ_s fixed for FWHM of the Gaussian pulses taking the values $\sigma = \tau = \{1, 2, 4, 8\} \times 20$ ns with $t_0^p = 0.525\tau$. The Rabi frequencies of the S and P pulses are fixed to $\Omega_s^0 = \Omega_p^0 = 4.915 \times 10^8$ rad/s; thus the Ly-α pulse energy is changing, Eq. (16).

that the range of the detuning δ_p that produces population in the $2S$ state increases by increasing the Rabi frequency Ω_0 and has a linewidth that is approximately linear in Ω_0 [29,30]. This will be important for controlling the width of the velocity distribution of the resulting $2S$ atoms from a wide thermal ensemble of initial $1S$ atoms that experiences Doppler detuning in Sec. III B.

The number of emitted photons during the decay process from the $2P$ state to the $1S$ state is useful in understanding the change in the velocity distribution of the hydrogen atoms. High-velocity atoms experience high Doppler detunings. Thus knowing the number of emitted photons at different detunings gives an idea of the amount of recoil experienced by each velocity class of the hydrogen atoms, Sec. III B. In the simulations it was observed that as the detuning goes to zero, the number of photons emitted during the whole STIRAP process approaches its smallest value. In Fig. 4 it can be seen that there are fewer photons emitted at zero P pulse detuning δ_p, at fixed Ω_p^0, for longer pulses durations. This happens because the STIRAP efficiency, at high decay rates, $\Gamma_0 > \Omega_0$ [12,17], improves for longer pulses durations, following the factor $\Omega_0^2 \times \tau/\Gamma$. However, at higher P pulse detuning the maximum number of emitted photons was observed to be higher for longer pulses durations, τ. This is because at high P pulse detuning δ_p, almost no transfer to the $2S$ state occurs and most of the electrons that make it to the $2P$ level decay back to the $1S$ level, emitting more photons in the process. Thus, for longer pulse durations, the atoms have enough time to be excited to the $2P$ level and decay to the $1S$ level multiple times.

The dependence of the emitted photons on the Rabi frequency $\Omega_s^0 = \Omega_p^0$ was observed to be similar to the dependence on the pulse duration. At zero P pulse detuning, the number of emitted photons decreases by increasing the pulse energy, i.e., improving the STIRAP adiabaticity. However, the difference was that the maximum number of emitted photons has a ceiling value that cannot be exceeded, independent of how much the Rabi frequencies are increased. That maximum

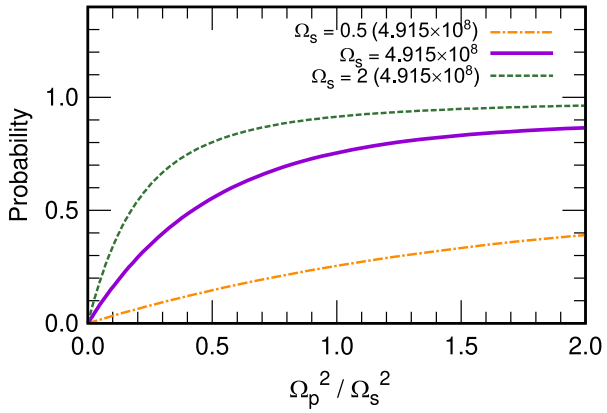

FIG. 5. The transfer probability into the $2S_d$ state as Ω_p^0 is varied while keeping Ω_s^0 fixed at zero pulse detunings. The transfer probability is linear in $(\Omega_p^0)^2$ for small $(\Omega_p^0)^2/(\Omega_s^0)^2$.

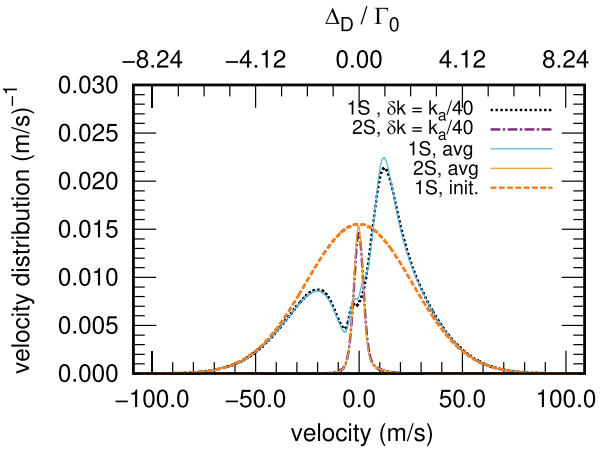

FIG. 6. The velocity distribution of the hydrogen atoms in the $1S$ and the $2S$ levels at $T = 80$ mK using the pulse parameters at the beginning of Sec. III A. The solid cyan and orange curves are produced using the averaged approximation, while the dotted black and dot-dashed purple curves are produced using the quantized approach developed in Sec. II B with momentum spacings $\delta k = k_\alpha/40$, with k_α being the wave number of the Ly-α pulse. The dashed orange curve is the initial Gaussian distribution of the hydrogen atoms before STIRAP. The upper x axis is the Doppler detuning $\Delta_D = \vec{v}\cdot\vec{k}_\alpha$ in units of the decay rate Γ_0, Appendixes B and A 2.

photon number is proportional to the number of possible excitation cycles to the $2P$ state that the system can go through over the pulse duration, thus proportional to $\tau\Gamma_0$. Finally, it is worth noting that when the energy in the pulse is kept fixed and the Rabi frequencies are changed with the pulse duration following Eq. (20), then neither the transfer efficiency nor the number of emitted photons, at zero pulses detunings, vary much by changing the pulses duration. The reasoning for this is that, for the STIRAP efficiency, the dependence on the pulses duration cancels out from the efficiency factor $\Omega_0^2\times\tau/\Gamma > 1$ [12]. We observed that as the pulses durations increased, the maximum population in the $2P$ level decreased, but the length of time it remained populated increased, resulting in almost the same number of emitted photons.

Increasing the peak Rabi frequencies of the STIRAP pulses increases the probability of population transfer to the $2S$ level [31] as observed in Figs. 3 and 5. For small Ω_p^0/Ω_s^0, the final probability to be in the $2S$ state increases linearly with $(\Omega_p^0)^2$, keeping Ω_s^0 fixed as shown in Fig. 5. The peak Rabi frequency of the Gaussian P pulse Ω_p^0 can be controlled through the energy in the pulse $\mathcal{E}$, the duration of the pulse τ, or the waist of the Gaussian pulse w_0 [32] with

$$\Omega_p^0 \propto \frac{\sqrt{\mathcal{E}}}{w_0\sqrt{\tau}}. \tag{16}$$

For a single atom that is fixed in space, it is irrelevant which of the two parameters $\{w_0, \mathcal{E}\}$ is used to tune Ω_p^0. However, when the decrease of the intensity of the Gaussian P pulse over the spacial extent of the atoms is accounted for in Sec. III B 2, the effects of changing the P pulse energy and its waist will not be equivalent; see Fig. 9.

B. STIRAP for a thermal ensemble

In this section we start with a thermal distribution of hydrogen atoms. This removes one of the idealizations of the previous section and leads to dependencies more relevant for experiments. Atoms are initialized from a Maxwell-Boltzmann distribution with the initial probability that a hydrogen atom has a momentum $\hbar k$ given by

$$\vartheta(k) = \frac{\hbar}{m_{\rm H}}\sqrt{\frac{m_{\rm H}}{2\pi\kappa_B T}}\exp\left(\frac{-\hbar^2k^2}{2m_{\rm H}\kappa_B T}\right), \tag{17}$$

where $m_{\rm H}$ is the mass of the hydrogen atom, κ_B is the Boltzmann constant, and T is the temperature.

1. *Velocity distribution of produced hydrogen atoms*

In Fig. 6 we initialized the hydrogen atoms at a temperature of 80 mK and let the system evolve under the master equation (5) using the pulse parameters discussed at the beginning of Sec. III A. We compared the final distribution of the hydrogen atoms in the $1S$ and the $2S$ states using the approaches discussed in Sec. II B in Fig. 6. There is a slight difference in the hydrogen atoms distribution in the $1S$ state compared to the results from applying the averaged approach and the quantized approach. However, the two approaches give similar results for the $2S$ velocity distribution. We have checked that the result of the quantized approach has converged by comparing the results using two momentum grids with $\delta k = k_\alpha/10$ and $\delta k = k_\alpha/40$.

There are two key points when studying the velocity distribution of the hydrogen atoms in the $2S$ level resulting from the STIRAP process. Firstly, when the STIRAP process occurs, the hydrogen atom absorbs a photon with momentum $\hbar k_\alpha$ leading to momentum change of the atom. Secondly, since the atoms at nonzero velocities experience Doppler detuning, only the atoms near the velocity that has zero net detuning $\bar{\Delta} = \Delta' + \vec{v}\cdot\vec{k} = 0$ experience appreciable population transfer from the STIRAP. In Fig. 6 the initial hydrogen atoms ensemble was at a temperature $T = 80$ mK; the percentage of atoms transferred to the $2S$ state is approximately 9.6%.

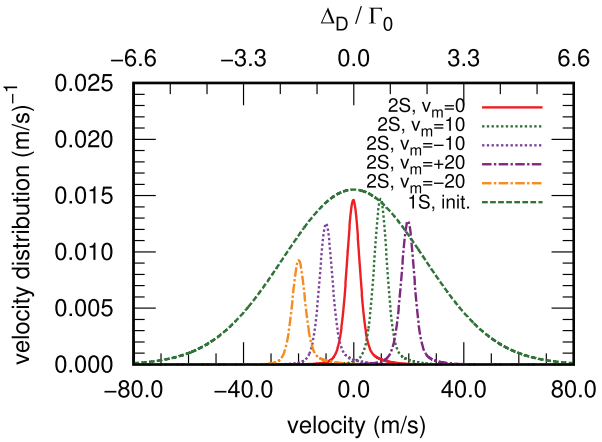

FIG. 7. The velocity distribution of the hydrogen atoms in the $2S$ level at $T = 80$ mK using the pulses parameters at the beginning of Sec. III A. Different detunings for the Ly-α pulse are used to produce hydrogen atoms in the $2S$ level with the peak velocities $\{-20, -10, 0, 10, 20\}$ m/s. The dashed green curve is the initial Gaussian distribution of the hydrogen atoms before STIRAP. The upper x axis is the Doppler detuning $\Delta_D = \vec{v} \cdot \vec{k}_\alpha$ in units of the decay rate Γ_0, Appendixes B and A 2.

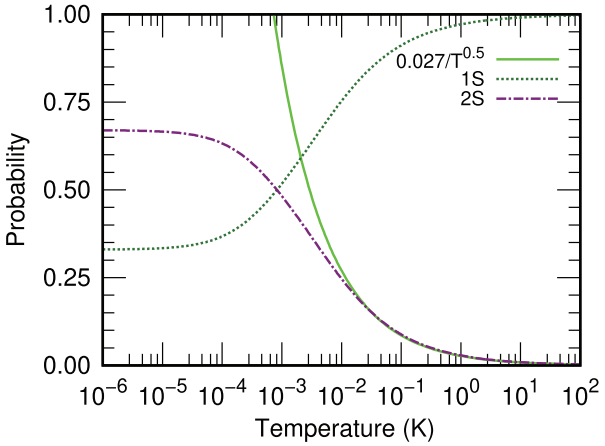

FIG. 8. The total probability of the hydrogen atoms being in the $1S$ and the $2S$ levels as a function of the initial temperature of the hydrogen atoms ensemble using the pulses parameters at the beginning of Sec. III A. The detuning Δ' in the Hamiltonian, Eq. (A6), is set to zero for all temperatures. We also plot the high-temperature asymptotic behavior curve $\propto 1/\sqrt{T}$.

That percentage is small, compared to the stationary atom ∼75%, because at $T = 80$ mK most of the atoms have a large Doppler detuning, taking most of them off resonance, and little transfer occurs. The width of the velocity distribution of the produced $2S$ atoms increases as the Rabi frequency increases as expected from the results in Fig. 3. After STIRAP, the $1S$ hydrogen atoms velocity distribution is a mixture of the high-velocity, highly detuned, $1S$ atoms of the initial Gaussian distribution, that did not absorb any photons, and the ones that got excited to the $2P$ state and then decayed back to the $1S$ level. The recoil the atoms experience when absorbing the Ly-α pulse gives them positive velocity kicks, which is seen in the decrease of the number of negative velocity atoms and the increase of positive velocity ones. This suggests that if consecutive pulses are used on the same sample, then sending alternating pulses from opposite directions could reduce the heating effects.

It is possible to pick the location of the peak of the final velocity of the hydrogen atoms in the $2S$ level as long as it is inside the thermal distribution by adjusting the pulse detuning Δ [33]; see Appendix A 2. In Fig. 6 we adjusted the detuning such that the peak of the hydrogen atoms in the $2S$ state after receiving the momentum kick would be at zero velocity using

$$\Delta' = \delta' = \hbar \frac{k_\alpha^2}{m_{\rm H}} \sim 0.27\Gamma_0. \tag{18}$$

We show the feasibility of controlling the peak velocity of the produced hydrogen atoms from the STIRAP process in Fig. 7. We use an initial ensemble at temperature $T = 80$ mK and by adjusting the detuning of the Ly-α pulse we produce hydrogen atoms in the $2S$ level with peak velocities $v_m = \{-20, -10, 0, 10, 20\}$ m/s. Since the atoms in the $2S$ level have received a velocity kick v_k from absorbing the Ly-α pulse, the peak of $2S$ atoms velocity distribution is proportional to the Gaussian Maxwell-Boltzmann distribution evaluated at $v_m - v_k$ instead of just v_m. This feature could be experimentally useful if a specific velocity of $2S$ atoms was desired.

In Fig. 8 we examine how the percentage of the atoms that end up in the different states changes as we change the temperature. We see that at high temperatures, the momentum range that gives a Doppler detuning within the STIRAP transfer domain $\sim[-\Omega_0 : \Omega_0]$ becomes small compared to $\kappa_B T$. Thus the factor $\exp(\frac{-\hbar^2 k^2}{2m_{\rm H}\kappa_B T})$ becomes almost unity, and the transfer rate dependence on the temperature varies as $\frac{1}{\sqrt{T}}$. For the pulses parameters discussed at the beginning of Sec. III A, this dependence was observed for temperatures higher than about $T = 10$ mK. For low temperatures, $T < 0.1$ mK, the thermal velocities become very small and the Doppler detuning becomes negligible, so one gets the high transfer rate observed for zero detuning in Sec III A. For instance, temperatures lower than $T = 0.01$ mK have a small initial velocity spread and approximately 66% of the atoms' population transfers to the $2S$ level with an average momentum $\hbar k_\alpha$. The reason why this rate is not exactly the ∼75% in Fig. 2 for stationary atoms is that here the atoms decaying from the $2P$ to the $1S$ level can experience high Doppler detuning due to the decay recoil not canceling out the momentum kick from absorbing the Ly-α. From our simulations, we find that increasing the Rabi frequency of the pulses does not change the overall dependence on the temperature; it only shifts the temperature at which the asymptotic $\propto 1/\sqrt{T}$ behavior starts. For instance, at 8 times the Rabi frequency, the transfer ratio becomes about 50% near $T = 100$ mK. We note here that cooling with optical molasses can get the hydrogen atoms to minimum temperatures of only a few millikelvins [34,35].

Although lower-temperature ensembles of hydrogen atoms produce a higher percentage of atoms in the $2S$ level, they are less tolerant to changes in detuning. For example, this is observed when comparing the percentage of atoms that transfer to the $2S$ level at the two temperatures $T = 1$ mK and

$T = 80\,\mathrm{mK}$. At zero detuning the lower-temperature ensemble transfers about 50% of the atoms to the $2S$ level, while the ensemble at $T = 80\,\mathrm{mK}$ transfers only about 10%. However, the lower-temperature ensemble has a width of only about one Γ_0, while the higher-temperature ensemble has a width almost three times as much. This happens because at higher temperatures the Maxwell-Boltzmann distribution velocity range is larger. Thus such atoms' Doppler detuning can cancel out the laser detuning, allowing for transitions at a larger laser detuning range.

2. *Including the spatial profile of the Ly-α pulse*

In this section, we remove the last idealization of Sec. III A and evaluate the number of $2S$ atoms taking into account the radial profile of the Ly-α beam. Since the Ly-α is typically a Gaussian beam in the radial direction, not all trapped atoms experience STIRAP with the same Rabi frequency Ω_p^0 due to the spatial dependence of the intensity, Eq. (20). However, the S pulse is constant in the radial direction, which results in a pulse configuration different from that of perfect STIRAP and rather a STIRAP-like one. A sample of number density, ϕ, and length, L, would produce N hydrogen atoms in the $2S$ level with

$$N = nL\phi = L\phi \int_0^\infty 2\pi r P_{2S}(r) dr, \tag{19}$$

where n gives the number of atoms in the $2S$ level in units of m^2/pulse. We introduce n as a cross-section-like parameter since it is independent of the sample density and length. The $P_{2S}(r)$ is the transition probability into the $2S$ level by the end of the pulse duration, which depends on the specific Rabi frequency at radial distance, r, from the center of the path of the pulse,

$$\Omega_p^0(r) \propto e^{-r^2/w_0^2} \frac{\sqrt{\mathcal{E}}}{w_0\sqrt{\tau}}, \tag{20}$$

where the variation in the pulse waist is negligible over the sample size as the Rayleigh length is larger than 6 m for $w_0 > 0.5\,\mathrm{mm}$. A rough estimate for the parameter n could be obtained by multiplying the probability of transfer at a certain temperature by the beam area $\sim\pi w_0^2$. In Fig. 6, the transfer probability is about 9.6%, giving $n \sim 1.2\times10^{-6}$ which is close to the actual value of $\sim 0.9\times10^{-6}$ in Fig. 9.

In Fig. 9 we show the number of atoms in the $2S$ level as a function of the pulse waist for different pulse energies $\{1, 3, 5\}$ nJ. We see that even though the decrease in pulse waist increases, Ω_p^0, the number of transferred hydrogen atoms decreases as the waist decreases. This happens because the effective spatial extent of the pulse is of order w_0. Thus decreasing w_0 reduces the effective region where efficient STIRAP occurs. However, the large waist behavior could be understood by referring to Fig. 5, where for small Ω_p^0 and fixed Ω_s^0 the transfer probability is linear in $(\Omega_p^0)^2$. Thus, for large w_0, that is, small Ω_p^0, the radial integral of the probability with Ω_p^0 in Eq. (20) turns out to be independent of the waist. The dependence on the pulse energy could be understood in the same manner, where the number of transferred hydrogen atoms is approximately linear in the P pulse's energy at large waist. We investigated the velocity distribution of the $2S$ hydrogen atoms after including the spatial profile of the Ly-α pulse and got results similar to Fig. 7 with the same relative peak amplitudes and distribution linewidth.

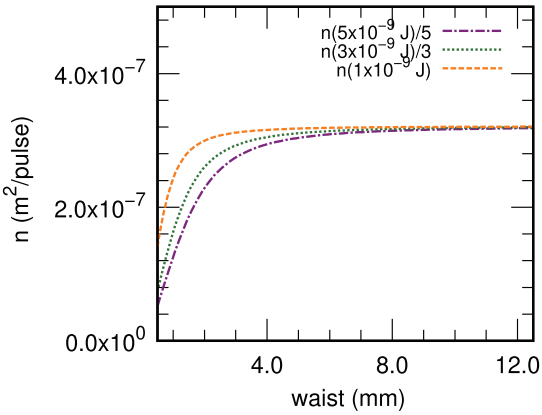

FIG. 9. The dependence of the number of hydrogen atoms transferred to the $2S$ level per pulse on the pulse waist for the Ly-α pulse energies $\{1, 3, 5\}$ nJ, temperature $T = 80\,\mathrm{mK}$ and S pulse Rabi frequency $\Omega_s^0 = 4.915\times10^8$ rad/s. The curves are scaled to show the linear dependence on the energy at large beam waist.

C. $1S_c \rightarrow 2S_c$ STIRAP in the presence of magnetic field

It is possible to transfer population into another hyperfine sublevel of the $2S$ level, namely, the $2S_c$ sublevel. This is achieved using a magnetic field to split the energy levels [25–27]. In Sec. II C we studied how the magnetic field affects the STIRAP Hamiltonian connecting the states $1S_c$ to $2S_c$. The magnetic field introduces a shift in the energy that increases as the magnetic field increases. We showed that this energy shift could be absorbed in the detuning in Eq. (15). For a magnetic field of 0.05 T that shift is about

$$\begin{aligned} 2B\frac{g_e e}{\hbar m_e} - E^{1S}(B) &= 11.12\Gamma_0, \\ E^{2S}(B) - E^{1S}(B) &= 7.85\Gamma_0, \end{aligned} \tag{21}$$

which shifts the energies of the states off resonance from the Ly-α pulse. A population transfer between the desired levels is achieved by adjusting the pulses detunings $\{\Delta, \delta\}$.

As discussed in Sec. II C, the main effects of introducing a magnetic field on the Hamiltonian would be the factor of $\beta_i(\mathrm{B})$ in the off-diagonal terms. For a magnetic field of 0.05 T these factors are $\beta_{1S}^2 = 0.854$ and $\beta_{2S}^2 = 0.995$ while for B 0.15 T they become $\beta_{1S}^2 = 0.974$ and $\beta_{2S}^2 = 0.999$. In treating the decay, only a β_{1S}^2 fraction of the atoms in the $2P$ state decay into the $1S_c$ state while the remaining fraction, $1 - \beta_{1S}^2$, decay to the untrappable $1S_a$ state. Thus a fraction $1 - \beta_{1S}^2$ of the atoms leaves the three-state subsystem $\{1S_c, 2P_a^\downarrow, 2S_c\}$. Since the magnetic fields of interest have the $1S_a$ state far off resonance, there is almost no transfer of population out of the $1S_a$ state. Since the factor β_{1S}^2 approaches unity as the magnetic field increases, the population leakage out of the subsystem decreases for larger magnetic fields. This is shown in Fig. 10(b) where the number of hydrogen atoms lost outside the subsystem is evaluated for different values of the magnetic field. The number of atoms decaying into the $1S_a$

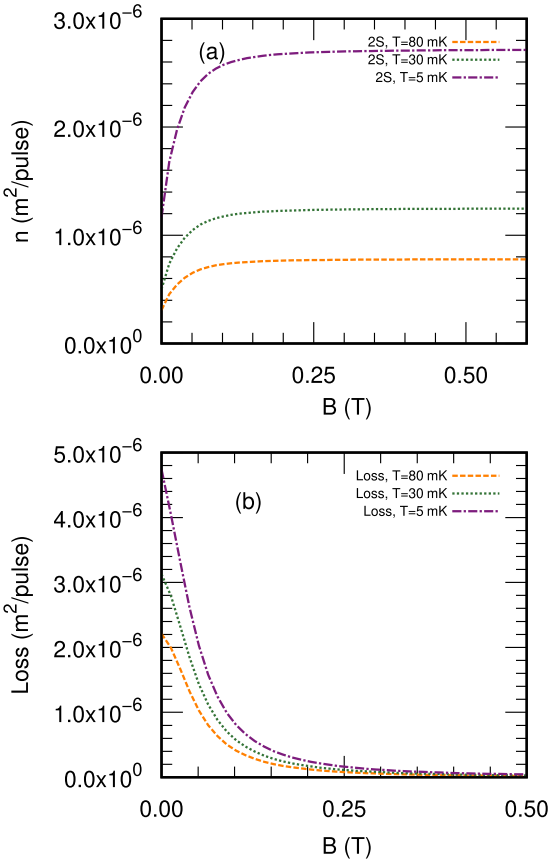

FIG. 10. The number of hydrogen atoms in the $2S_c$ state (a) as well as the number of atoms leaving the subspace $\{1S_c, 2P_a^{\downarrow}, 2S_c\}$ (b) as a function of the applied magnetic field with zero detunings at temperatures $T = \{5, 30, 80\}$ mK. The P pulse has a waist $w_0 = 2.0$ mm and an energy of 3 nJ.

state decreases about 10 times as the magnetic field increases from 0 to 0.15 T. Similarly, the presence of the magnetic field enhances the STIRAP transfer efficiency, as shown in Fig. 10(a) where the number of atoms moving to the $2S_c$ level more than doubled as the magnetic field increased from 0 to 0.15 T. Magnetic fields bigger than 0.15 T hardly improve the transfer rates, as β_{1S}^2 becomes almost unity. At lower temperatures the loss in population is higher for the same magnetic fields because the lower Doppler detuning experienced by the atoms at lower temperatures leads to more $1S_c$-$2P_a$ transitions.

Other than the loss in the population due to decaying with spin flip, the behavior of the system with a magnetic field is similar to that studied in the previous subsection. For instance, when varying the detuning, the transfer probability to the $2S$ level is the same as that without including a background magnetic field. The only difference is a slight decrease of the transfer rate to the $2S$ level in the presence of a magnetic field due to the loss of trapped atoms through decaying into the $1S_a$ state. However, as the magnetic field increases, β_{1S}^2 gets closer to unity and the system behaves like the closed three-state system discussed in the previous subsection.

IV. CONCLUSION

We investigate conditions for the validity of a general STIRAP procedure from the $1S$ to the $2S$ levels in the hydrogen atom. We utilize a Ly-α pulse for the $1S$-$2P$ coupling and a microwave pulse for the $2P$-$2S$ coupling. The stretched states $\{1S_d, 2P_a^{\uparrow}, 2S_d\}$ form a 3×3 closed lambda linkage between which the STIRAP process could be utilized without the need for an external magnetic field. We also show that by applying a magnetic field, the STIRAP process is also achievable between the states $\{1S_c, 2P_a^{\downarrow}, 2S_c\}$. We find that significant transfer rates through STIRAP occur when the detuning of the P pulse is approximately smaller than the maximum of the Rabi frequency. It is also observed that at a fixed microwave pulse's Rabi frequency, the transfer efficiency of STIRAP has a quadratic dependence on the Rabi frequency of the Ly-α pulse for small Rabi frequencies.

We study thermal ensembles of hydrogen atoms and their resulting velocity distribution after the STIRAP process. Atoms at temperatures of a few tens of millikelvins experience Doppler detunings of comparable order of magnitudes to the energies in the system. This Doppler detuning takes the atoms off resonance with the Ly-α pulse and thus affects the efficiency of the STIRAP. The transition probabilities into the $2S$ level are larger at lower temperatures and proportional to $\propto 1/\sqrt{T}$ for temperatures higher than 100 mK for P pulse Rabi frequency $\Omega_p^0 = 4.915\times10^8$ rad/s. The temperature at which the $1/\sqrt{T}$ dependence begins increases with increasing the Rabi frequency of the Ly-α pulse. We show that it is possible to control the peak velocity of the resulting hydrogen atoms in the $2S$ level by changing the Ly-α pulse's detuning.

We examine, taking into account the spatial Gaussian profile of the Ly-α pulse, the effect of changing the Ly-α pulse waist and energy on the number of $2S$ hydrogen atoms produced. Generally, increasing the Ly-α pulse energy increases the number of hydrogen atoms undergoing STIRAP. However, the number of atoms transferred through STIRAP increases with the pulse waist for small Ly-α beam waists. It then reaches a plateau where the increased area of the beam is countered by the decrease in the pulse intensity and increasing the waist has little effect. These findings assume that the pulses are not depleted by the atoms in the gas as well as that the trapped hydrogen atoms fill all the spatial extent of the Ly-α pulse.

Finally, we study the effects of applying an external magnetic field on the STIRAP process. We showthat the STIRAP process can be applied to transfer population between trappable states inside a magnetic field. For the states $\{1S_c, 2S_c\}$ increasing the magnetic field keeps the population in the desired trappable states by sending the other states off resonance with the microwave and Ly-α pulses. The branching ratio of the decay of the $2P_a^{\downarrow}$ into the trappable state $1S_c$ approaches unity as the magnetic field increases. Consequently, loss in hydrogen atoms through decaying into the untrappable $1S_a$ state decreases with increasing magnetic field. Thus it is possible to control the target states into which the STIRAP transfers the hydrogen atoms.

As discussed in Sec. III A we experiment with different possible parameters for the microwave pulse's configuration, and the ones used in the simulations are the optimal ones found. The Ly-α pulse is restricted to a Gaussian pulse for experimental purposes. Further STIRAP optimization techniques such as optimal pulse control and the stimulated

Raman exact passage (STIREP) [36–38] could be future research directions if needed.

ACKNOWLEDGMENTS

This work was supported by the U.S. National Science Foundation under Grant No. 2409162-PHY and Natural Sciences and Engineering Research Council of Canada, National Research Council of Canada, TRIUMF, and Canada Foundations for Innovations.

DATA AVAILABILITY

The data plotted in the figures are available in Ref. [39].

APPENDIX A: DERIVATION OF THE HAMILTONIAN

This Appendix shows the details of evaluating the STIRAP Hamiltonian used in this work, Eq. (6). First, we start by simplifying the expressions for the general matrix element connected through the electric field in Eq. (1). We apply the Wigner-Eckart theorem [22] to obtain the ratios between the different nonzero matrix elements connecting the hyperfine states of the $2P$ to those of the $1S$ and $2S$ levels.

1. Stationary atoms STIRAP Hamiltonian

We start with the wave function,

$$|\psi\rangle = c_1(t)e^{-i\varepsilon_1 t/\hbar}|1\rangle + c_2(t)e^{-i\varepsilon_2 t/\hbar}|2\rangle + c_3(t)e^{-i\varepsilon_3 t/\hbar}|3\rangle, \tag{A1}$$

with the states corresponding to the $1S$, $2P$, and $2S$ states in ascending order. The coupling to the Ly-α and the microwave fields, Eq. (1), leads to the evolution of the amplitudes in the states as follows:

$$\begin{aligned} i\dot{c}_1 &= -e^{i(\omega_\alpha-\omega_{12})t}\Omega_p c_2/2, \\ i\dot{c}_2 &= -e^{-i(\omega_\alpha-\omega_{12})t}\Omega_p^* c_1/2 - e^{-i(\omega_s-\omega_{32})t}\Omega_s^* c_3/2, \\ i\dot{c}_3 &= -e^{i(\omega_s-\omega_{32})t}\Omega_s c_2/2, \end{aligned} \tag{A2}$$

where the Rabi frequencies from the P and S pulses are given by

$$\begin{aligned} \Omega_p &= -\frac{eE_p^0}{\hbar\sqrt{2}}\langle 1|x-iy|2\rangle = -eE_p^0\langle 1|r_-|2\rangle/\hbar, \\ \Omega_s &= -\frac{eE_s^0}{\hbar\sqrt{2}}\langle 3|x-iy|2\rangle = -eE_s^0\langle 3|r_-|2\rangle/\hbar, \end{aligned} \tag{A3}$$

with transition frequencies $\omega_{12} = \varepsilon_2 - \varepsilon_1$ and $\omega_{32} = \varepsilon_2 - \varepsilon_3$. The counterpropagating terms involving Ω_p^* as well as the off-resonant ones involving E_s^0 were omitted in the equation for $\dot{c}_1$ and their corresponding ones in the time derivative of c_2. Similar terms were omitted in the time derivative of c_3 and their corresponding ones in c_2. The final step is to redefine $c_2 \to e^{i\Delta t}c_2$ and $c_3 \to e^{i\delta t}c_3$, with $\Delta = \omega_\alpha - \omega_{12}$ and $\delta = \omega_\alpha - \omega_s - \omega_{12} + \omega_{32}$, to get the simplified expressions:

$$\begin{aligned} i\dot{c}_1 &= -\tfrac{1}{2}\Omega_p c_2, \\ i\dot{c}_2 &= -\Delta c_2 - \tfrac{1}{2}\Omega_p^* c_1 - \tfrac{1}{2}\Omega_s c_3, \\ i\dot{c}_3 &= -\delta c_3 - \tfrac{1}{2}\Omega_s^* c_2. \end{aligned} \tag{A4}$$

This reproduces the Hamiltonian in Eq. (6) with Δ and δ being the single-photon and the two-photon detunings, respectively.

2. Including the atom's motion effects on the STIRAP Hamiltonian

Here we present the STIRAP Hamiltonian when the center of mass motion is taken into account. For the treatment here, we let the initial hydrogen atom be in the state $|i\rangle = 1S_d \otimes |\vec{k}\rangle$, where the first part is the internal state $1S$ and the second part is the state of the center of mass having momentum $\hbar\vec{k}$. After absorbing the Ly-α pulse, the center of mass would gain a momentum kick of $\hbar\vec{k}_\alpha = \hbar 2\pi/(121.6\times10^{-9})$ kg m/s or equivalently a velocity shift of $\vec{v}_k \sim 3.25\hat{k}_\alpha$ m/s. Since the wavelength of the photon that couples the $2P$ and the $2S$ states is orders of magnitude larger than that of the Ly-α, we assume here that the $2P$ and the $2S$ states have the same momentum of $\hbar(\vec{k}+\vec{k}_\alpha)$. Thus, after including the center of mass kinetic energy, the Hamiltonian becomes

$$H^k = \hbar\begin{pmatrix} \frac{\hbar k^2}{2m_p} & -\frac{\Omega_p}{2} & 0 \\ -\frac{\Omega_p}{2} & -\Delta + \hbar\frac{k^2+2\vec{k}\cdot\vec{k}_\alpha+k_\alpha^2}{2m_p} & -\frac{\Omega_s}{2} \\ 0 & -\frac{\Omega_s}{2} & -\delta + \hbar\frac{k^2+2kk_\alpha+k_\alpha^2}{2m_p} \end{pmatrix}. \tag{A5}$$

To better understand this Hamiltonian, we shift the energy by subtracting $\hbar^2k^2/2m_p$ from the diagonal and identify $2\vec{k}\cdot\vec{k}_\alpha/2m_p$ as the usual Doppler detuning $\Delta_D = \vec{v}\cdot\vec{k}_\alpha$. Thus we end up with the Hamiltonian:

$$H = \hbar\begin{pmatrix} 0 & -\frac{\Omega_p}{2} & 0 \\ -\frac{\Omega_p}{2} & -\Delta' + \vec{v}\cdot\vec{k}_\alpha & -\frac{\Omega_s}{2} \\ 0 & -\frac{\Omega_s}{2} & -\delta' + \vec{v}\cdot\vec{k}_\alpha \end{pmatrix}. \tag{A6}$$

This is the full Hamiltonian that includes the effect of having a moving center of mass for the hydrogen atom. Note that the factor $\hbar\frac{k_\alpha^2}{2m_p}$ has a value of approximately one-eighth of a Γ_0 and was absorbed in the definition of the detuning such that

$$\begin{aligned} \Delta' &= \Delta - \hbar\frac{k_\alpha^2}{2m_p}, \\ \delta' &= \delta - \hbar\frac{k_\alpha^2}{2m_p}. \end{aligned} \tag{A7}$$

Thus the main change in the Hamiltonian would be to include the Doppler detuning in the relevant diagonal terms.

APPENDIX B: DECAY CHANNELS AND RATES

The decay rates Γ_n, from the different $2P$ states to the possible hyperfine levels of $1S$, are

$$\begin{aligned} \Gamma_1(|2,2\rangle \to |1\rangle) &= \Gamma_0, \\ \Gamma_2(|2,1\rangle \to |1\rangle) &= \Gamma_0/2, \\ \Gamma_3(|2,1\rangle \to |+\rangle) &= \Gamma_0/2, \\ \Gamma_4(|2,0\rangle \to |1\rangle) &= 2\Gamma_0/3, \\ \Gamma_5(|2,0\rangle \to |+\rangle) &= \Gamma_0/6, \\ \Gamma_6(|2,0\rangle \to |-1\rangle) &= \Gamma_0/6, \end{aligned}$$

$$\begin{aligned}
\Gamma_7(|1,1\rangle \to |1\rangle) &= \Gamma_0/6,\\
\Gamma_8(|1,1\rangle \to |+\rangle) &= \Gamma_0/6,\\
\Gamma_9(|1,1\rangle \to |-\rangle) &= 2\Gamma_0/3,\\
\Gamma_{10}(|1,0\rangle \to |1\rangle) &= 2\Gamma_0/3,\\
\Gamma_{11}(|1,0\rangle \to |-\rangle) &= \Gamma_0/6,\\
\Gamma_{12}(|1,0\rangle \to |-1\rangle) &= \Gamma_0/6,
\end{aligned} \tag{B1}$$

where the notation is such that $\Gamma_n(|F, m_F\rangle \to |f\rangle)$ is the decay rate from the $2P$ state having total angular momentum F, with z component angular momentum m_F, to the $1S$ hyperfine state $|f\rangle$. The hyperfine $1S$ states are such that $(|1\rangle, |+\rangle, |-1\rangle)$ form the triplet subspace with decreasing z component's angular momentum and the $|-\rangle$ is the singlet state. The value of Γ_0 is found analytically using the quantization of the electric field [23] and experimentally [40] it has the value $\Gamma_0 = 6.27\times10^8\ \mathrm{s}^{-1}$.

We do not include the branching ratio to the $2S$ states through spontaneous photon emission because the decay rate is about 15 orders of magnitude smaller than that from the $2P$ levels to the $1S$ levels.

[1] C. G. Parthey, A. Matveev, J. Alnis, B. Bernhardt, A. Beyer, R. Holzwarth, A. Maistrou, R. Pohl, K. Predehl, T. Udem, T. Wilken, N. Kolachevsky, M. Abgrall, D. Rovera, C. Salomon, P. Laurent, and T. W. Hänsch, Improved measurement of the hydrogen $1S$-$2S$ transition frequency, Phys. Rev. Lett. **107**, 203001 (2011).

[2] M. Niering, R. Holzwarth, J. Reichert, P. Pokasov, T. Udem, M. Weitz, T. W. Hänsch, P. Lemonde, G. Santarelli, M. Abgrall *et al.*, Measurement of the hydrogen $1s$-$2s$ transition frequency by phase coherent comparison with a microwave cesium fountain clock, Phys. Rev. Lett. **84**, 5496 (2000).

[3] C. J. Baker, W. Bertsche, A. Capra, C. Carruth, C. L. Cesar, M. Charlton, A. Christensen, R. Collister, A. C. Mathad, S. Eriksson *et al.*, Precision spectroscopy of the hyperfine components of the $1s$–$2s$ transition in antihydrogen, Nat. Phys. **21**, 201, (2025).

[4] M. Ahmadi, B. X. R. Alves, C. J. Baker, W. Bertsche, E. Butler, A. Capra, C. Carruth, C. L. Cesar, M. Charlton, S. Cohen *et al.*, Observation of the hyperfine spectrum of antihydrogen, Nature (London) **548**, 66 (2017).

[5] M. Ahmadi, B. X. R. Alves, C. J. Baker, W. Bertsche, E. Butler, A. Capra, C. Carruth, C. L. Cesar, M. Charlton, S. Cohen *et al.*, Observation of the $1S$-$2S$ transition in trapped antihydrogen, Nature (London) **541**, 506 (2017).

[6] M. Ahmadi, B. X. R. Alves, C. J. Baker, W. Bertsche, A. Capra, C. Carruth, C. L. Cesar, M. Charlton, S. Cohen, R. Collister *et al.*, Characterization of the $1S$-$2S$ transition in antihydrogen, Nature (London) **557**, 71 (2018).

[7] A. Matveev, C. G Parthey, K. Predehl, J. Alnis, A. Beyer, R. Holzwarth, T. Udem, T. Wilken, N. Kolachevsky, M. Abgrall *et al.*, Precision measurement of the hydrogen $1S$-$2S$ frequency via a 920-km fiber link, Phys. Rev. Lett. **110**, 230801 (2013).

[8] C. Ø. Rasmussen, N. Madsen, and F. Robicheaux, Aspects of $1S$-$2S$ spectroscopy of trapped antihydrogen atoms, J. Phys. B **50**, 184002 (2017).

[9] C. E. Carroll and F. T. Hioe, Coherent population transfer via the continuum, Phys. Rev. Lett. **68**, 3523 (1992).

[10] T. Nakajima, M. Elk, J. Zhang, and P. Lambropoulos, Population transfer through the continuum, Phys. Rev. A **50**, R913 (1994).

[11] L. P. Yatsenko, R. G. Unanyan, K. Bergmann, T. Halfmann, and B. W. Shore, Population transfer through the continuum using laser-controlled stark shifts, Opt. Commun. **135**, 406 (1997).

[12] P. A. Ivanov, N. V. Vitanov, and K. Bergmann, Spontaneous emission in stimulated Raman adiabatic passage, Phys. Rev. A **72**, 053412 (2005).

[13] A. E. Kramida, A critical compilation of experimental data on spectral lines and energy levels of hydrogen, deuterium, and tritium, At. Data Nucl. Data Tables **96**, 586 (2010).

[14] V. S. Ivanov, Y. V. Rozhdestvensky, and K.-A. Suominen, Theory of robust subrecoil cooling by stimulated Raman adiabatic passage, Phys. Rev. A **85**, 033422 (2012).

[15] V. S. Ivanov, Y. V. Rozhdestvensky, and K.-A. Suominen, Robust two-dimensional subrecoil Raman cooling by adiabatic transfer in a tripod atomic system, Phys. Rev. A **86**, 033409 (2012).

[16] T. A Vovk, S. S. Rudyi, A. V. Ivanov, E. Y. Perlin, and Y. V. Rozhdestvensky, Features of laser cooling of Yb-doped fluorite nanocrystals using coherent population transfer techniques, in *Nonlinear Optics and Applications XI* (SPIE, Bellingham, WA, 2019), Vol. 11026, pp. 131–137.

[17] N. V. Vitanov, A. A. Rangelov, B. W. Shore, and K. Bergmann, Stimulated Raman adiabatic passage in physics, chemistry, and beyond, Rev. Mod. Phys. **89**, 015006 (2017).

[18] M. Diermaier, C. B. Jepsen, B. Kolbinger, C. Malbrunot, O. Massiczek, C. Sauerzopf, M. C. Simon, J. Zmeskal, and E. Widmann, In-beam measurement of the hydrogen hyperfine splitting and prospects for antihydrogen spectroscopy, Nat. Commun. **8**, 15749 (2017).

[19] M. Fujiwara, T. Momose, A. Capra, R. Collister, T. Friesen, D. Gill, A. Evans, M. Hayden, A. Khramov, S. Menary *et al.*, Demonstration of laser cooling of antihydrogen and its applications in precision antimatter experiments, in *APS Division of Atomic, Molecular and Optical Physics Meeting Abstracts* (APS, College Park, MD, 2020), Vol. 2020, p. J07-006.

[20] A. Capra *et al.*, Observation of gravitational free-fall of antimatter with ALPHA-g at CERN and future development with HAICU at TRIUMF, in *APS Division of Atomic, Molecular and Optical Physics Meeting Abstracts* (APS, College Park, MD, 2024), Vol. 2024, p. Y03-001.

[21] K. Bergmann, N. V. Vitanov, and B. W. Shore, Perspective: Stimulated Raman adiabatic passage: The status after 25 years, J. Chem. Phys. **142**, 170901 (2015).

[22] H. Georgi, *Lie Algebras in Particle Physics: From Isospin to Unified Theories* (Taylor & Francis, Abingdon, UK, 2000).

[23] R. Shankar, *Principles of Quantum Mechanics* (Springer Science & Business Media, Berlin, 2012).

[24] K. Milton and J. Schwinger, *Classical Electrodynamics* (CRC Press, Boca Raton, FL, 2024).

[25] J. Martin, B. W. Shore, and K. Bergmann, Coherent population transfer in multilevel systems with magnetic sublevels. II. Algebraic analysis, Phys. Rev. A **52**, 583 (1995).

[26] J. Martin, B. W. Shore, and K. Bergmann, Coherent population transfer in multilevel systems with magnetic sublevels. III. Experimental results, Phys. Rev. A **54**, 1556 (1996).

[27] B. W. Shore, J. Martin, M. P. Fewell, and K. Bergmann, Coherent population transfer in multilevel systems with magnetic sublevels. I. Numerical studies, Phys. Rev. A **52**, 566 (1995).

[28] N. V. Vitanov and S. Stenholm, Analytic properties and effective two-level problems in stimulated Raman adiabatic passage, Phys. Rev. A **55**, 648 (1997).

[29] N. V. Vitanov, M. Fleischhauer, B. W. Shore, and K. Bergmann, in *Coherent Manipulation of Atoms Molecules By Sequential Laser Pulses*, edited by B. Bederson and H. Walther, Advances in Atomic, Molecular, and Optical Physics Vol. 46 (Academic Press, London, 2001), pp. 55–190.

[30] M. V. Danileiko, V. I. Romanenko, and L. P. Yatsenko, Landau-zener transitions and population transfer in a three-level system driven by two delayed laser pulses, Opt. Commun. **109**, 462 (1994).

[31] K. S. Kumar, A. Vepsäläinen, S. Danilin, and G. S. Paraoanu, Stimulated Raman adiabatic passage in a three-level superconducting circuit, Nat. Commun. **7**, 10628 (2016).

[32] O. Svelto, *Principles of Lasers* (Springer, Berlin, 2010), Vol. 1.

[33] M. G. Raizen, D. Budker, S. M. Rochester, J. Narevicius, and E. Narevicius, Magneto-optical cooling of atoms, Opt. Lett. **39**, 4502 (2014).

[34] P. H. Donnan, M. C. Fujiwara, and F. Robicheaux, A proposal for laser cooling antihydrogen atoms, J. Phys. B **46**, 025302 (2013).

[35] S. J. Walsh, C. Rasmussen, and F. Robicheaux, Simulated optical molasses cooling of trapped antihydrogen, J. Phys. B: Atom. Mol. Opt. Phys. **58**, 045202 (2025).

[36] D. Stefanatos and E. Paspalakis, Optimal shape of stirap pulses for large dissipation at the intermediate level, Quantum Inf. Proc. **20**, 391 (2021).

[37] X. Laforgue, G. Dridi, and S. Guérin, Optimal robust stimulated Raman exact passage by inverse optimization, Phys. Rev. A **105**, 032807 (2022).

[38] K. Liu, D. Sugny, X. Chen, and S. Guérin, Optimal pulse design for dissipative-stimulated Raman exact passage, Entropy **25**, 790 (2023).

[39] A. K. Amer, A. Capra, T. Friesen, M. C. Fujiwara, T. Momose, C. So, and F. Robicheaux, Data for: STIRAP simulations from the 1S to the 2S states for Hydrogen/Antihydrogen atoms, Purdue University Research Repository (2025).

[40] W. S. Bickel and A. S. Goodman, Mean lives of the $2p$ and $3p$ levels in atomic hydrogen, Phys. Rev. **148**, 1 (1966).